Knockdown Proteomics Reveals USP7 as a Regulator of Cell-Cell Adhesion in Colorectal Cancer *via* AJUBA

Authors

Ahood Al-Eidan, Ben Draper, Siyuan Wang, Brandon Coke, Paul Skipp, Yihua Wang, and Rob M. Ewing

Correspondence

rob.ewing@soton.ac.uk

In Brief

The deubiquitinase, USP7, regulates the abundance of cancer-associated proteins and is a key target in multiple types of tumor. Using USP7 knockdown coupled to label-free proteomics in a USP7-dependent cancer colorectal cell-line, new interaction partners of USP7 can be identified. These include Ajuba, a cell-cell adhesion scaffold protein identified as a USP7 interaction partner, thereby mediating the regulation of cell-cell adhesion by USP7.

Graphical Abstract

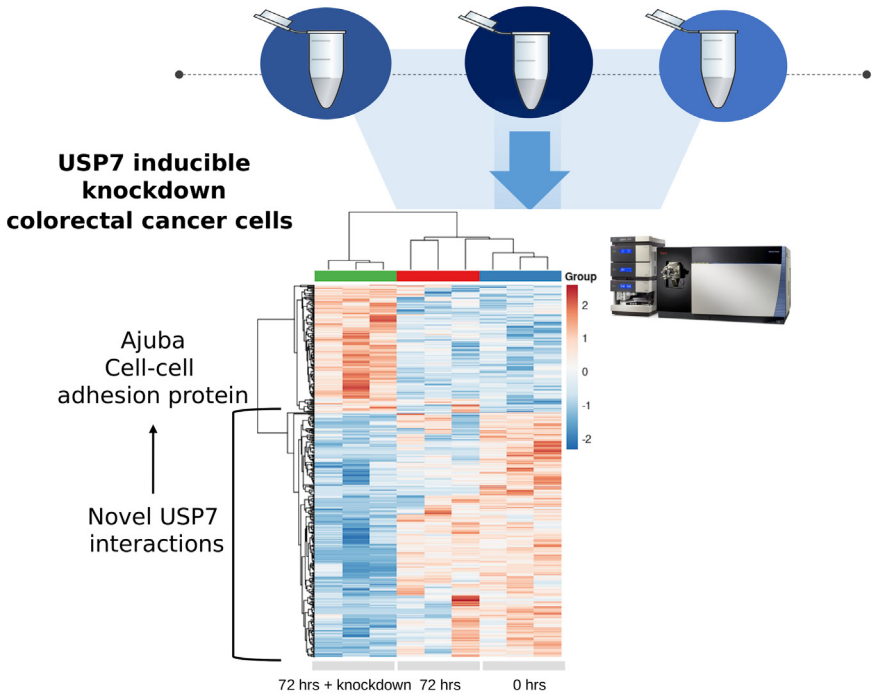

Highlights

- The deubiquitinase, USP7, is a key cancer target in many solid tumors.
- Knockdown proteomics can reveal novel USP7 interaction partners.
- USP7 interacts with Ajuba and thereby regulates cell-cell adhesion.

2024, Mol Cell Proteomics *23*(*12*), 100878

https://doi.org/10.1016/j.mcpro.2024.100878

Knockdown Proteomics Reveals USP7 as a Regulator of Cell-Cell Adhesion in Colorectal Cancer *via* AJUBA

Ahood Al-Eidan[1,2], Ben Draper[1], Siyuan Wang[1], Brandon Coke[1], Paul Skipp[1], Yihua Wang[1], and Rob M. Ewing[1,*]

Ubiquitin-specific protease 7 (USP7) is implicated in many cancers including colorectal cancer in which it regulates cellular pathways such as Wnt signaling and the P53–MDM2 pathway. With the discovery of small-molecule inhibitors, USP7 has also become a promising target for cancer therapy and therefore systematically identifying USP7 deubiquitinase interaction partners and substrates has become an important goal. In this study, we selected a colorectal cancer cell model that is highly dependent on USP7 and in which USP7 knockdown significantly inhibited colorectal cancer cell viability, colony formation, and cell-cell adhesion. We then used inducible knockdown of USP7 followed by LC-MS/MS to quantify USP7-dependent proteins. We identified the Ajuba LIM domain protein as an interacting partner of USP7 through co-IP, its substantially reduced protein levels in response to USP7 knockdown, and its sensitivity to the specific USP7 inhibitor FT671. The Ajuba protein has been shown to have oncogenic functions in colorectal and other tumors, including regulation of cell-cell adhesion. We show that both knockdown of USP7 or Ajuba results in a substantial reduction of cell-cell adhesion, with concomitant effects on other proteins associated with adherens junctions. Our findings underlie the role of USP7 in colorectal cancer through its protein interaction networks and show that the Ajuba protein is a component of USP7 protein networks present in colorectal cancer.

There has been rapidly increasing interest in the role of deubiquitinating enzymes (DUBs) in many types of tumor including colorectal cancer (CRC) (1). DUB proteins are proteases that reverse E3 ligase activity by cleaving a single ubiquitin, polyubiquitin chains or ubiquitin-like modifications on target proteins (2–4). This role of DUBs is similar to the regulatory role of the phosphatases in a kinase/phosphatase pathway (3). There are nearly 100 DUBs in the human genome, grouped into five families: ubiquitin-specific protease (USP), OUT, UCH, Josephin (cysteine proteases), and JAMM (a family of metalloproteases); DUBs have high specificity for ubiquitin. Different DUBs have different domains for the protein–protein interactions, substrate specificity, and cellular localization. Quantitative studies of multiple aspects of DUBs, including protein activity, protein network, and genetic studies, have discovered new DUB functions in both humans and yeast (3).

Deubiquitination is a regulatory process involved in multiple cell functions, such as cell cycle regulation (5), gene expression (6), and DNA repair (7). Moreover, mutations in many DUBs proteins have been implicated in various types of disease, including cancer and neurological disorders (8, 9). Despite it being evident that DUBs are critical to cell function, the targets and regulation processes of most DUB members have yet to be elucidated.

The largest DUB family is USP, which is comprised of more than 50 USP different deubiquitinating enzymes in humans and 16 UBPs in yeast (10). USPs have essential roles in protein regulation and function; disruption of their roles could lead to cancer progression. Thus, USP proteins have been targeted with anti-tumor chemotherapeutics (11). As a therapeutic strategy for cancer, drugs that target DUBs are predicted to be well tolerated (12). The structure of multiple DUBs in the USP/UBP class including USP7 have been characterized; this has enabled identification of the method of molecular recognition (ubiquitin or ubiquitin aldehyde-complexed) used by these proteases in their active state (13). The ubiquitin recognition mechanism is the same for the USP/UBP class, which show homology in their catalytic sites only (12) and has interaction domains in their insertions and terminal extensions (3). These features provide USP with high selectivity for its targets.

USP7 is one member of the of USP family that due to its functional importance has been quite extensively studied. Through its binding partners and substrates, USP7 plays fundamental roles in diverse cellular and biological processes, such as DNA repair, cell cycle, epigenetic regulation, and tumor suppression (14). Thus, mapping the USP7 network may

From the [1]School of Biological Sciences, Faculty of Environmental and Life Sciences, University of Southampton, Southampton, United Kingdom; [2]Department of Biology, College of Sciences, Imam Abdulrahman Bin Faisal University, Dammam, Saudi Arabia
*For correspondence: Rob M. Ewing, rob.ewing@soton.ac.uk.

https://doi.org/10.1016/j.mcpro.2024.100878

lead to discovering new cellular functions of USP7 that are implicated in CRC. USP7 is overexpressed in many cancers, including colorectal in which it has been shown to stabilize a number of proteins that promote tumorigenesis in diverse process such as enhanced proliferation, increased angiogenesis, and metastasis (15). USP7 promotes CRC growth by upregulating various cellular pathways, including Wnt/β-catenin signaling (16) and p53–Mdm2 pathway (17, 18). Finally, USP7 is one of the genes identified and combined to form a prognostic mutation panel in stage II and III CRC (19).

Despite the rapidly increasing number of USP7-related studies, relatively little is known about how USP7 regulates other key cancer-related pathways such as cell-cell adhesion, an important regulator of key tumor processes including epithelial-mesenchymal transition and metastasis. In this study, we used an inducible knockdown model of USP7 in CRC cells to identify new potential interaction partners, substrates, and ultimately functions, for USP7 in CRC. To identify potential new substrates and partners of USP7, we applied a quantitative label-free LC-MS/MS proteomics approach. First, we demonstrated that the inhibition of USP7 significantly reduced cell viability, cell proliferation, and cell-cell adhesion in 2D and 3D cultures. We then selected an appropriate USP7-sensitive cell-line by mining whole genome knockout studies and used an inducible knockout of USP7 in this cell-line to perform an LC-MS/MS screen for USP7-dependent proteins. From these results, we identified the LIM domain protein Ajuba as a novel interaction partner for USP7. We then used both cell-based and molecular approaches to investigate the role of Ajuba. Using Co-IP and knockdown, we show that Ajuba interacts with USP7 and that Ajuba protein levels are dependent on USP7. With Ajuba's known roles in cell adhesion, we next showed that knockdown of either USP7 or Ajuba in dispase-treated cell-cultures significantly enhanced loss of cell adhesion. We also showed that N-cadherin and E-cadherin levels are reduced in USP7 (and partially in Ajuba) knockdown cells albeit with no evidence of direct interaction between USP7 and the cadherins. In summary, we have identified Ajuba as a novel interaction partner of USP7 that mediates USP7 functional regulation of cell-cell adhesion in CRC cells.

EXPERIMENTAL PROCEDURES

Maintenance of Cell Lines

The CRC cell-line, HCT116, was cultured in McCoy's 5A media (Life Technologies, 26600023). LS174T cells were obtained from SIGMA-ALDRICH (8706040-1VL) and were cultured in Eagle's Minimum Essential Medium (ATCC 30-2003). LS174T cells are colon carcinoma cells carrying a pTER-USP7 shRNA construct and a Tet repressor-construct (indicated as LS88) (provided by Professor Madelon Maurice, University Medical Center Utrecht) (20). These cell lines were cultured in the RPMI media (Life Technologies, 6187010) and selected by (blasticidin 10 μg/ml (Invivo Gen, ant-bl-05) and zeocin 500 μg/ml (Invivo Gen, ant-zn-05)). Producing clones were stimulated for siRNA production by the addition of doxycycline (1 μg/ml) (Sigma, D9891-1G) for 24 h, 48 h and examined by Western blotting to downregulate the endogenous USP7. DLD-1 cell lines were regularly maintained in RPMI media (Life Technologies, 6187010), whereas HEK293T human embryonic kidney cells were routinely cultured in Dulbecco's Modified Eagle's Medium (Thermo Fisher Scientific). All cells were cultured in media supplemented with 10% fetal bovine serum and 1% streptomycin-penicillin at 37 °C in CO_2 incubator (5% CO_2) and were regularly tested for *mycoplasma*. All of the CRC cell-lines used (LS88, LS174T, DLD-1, HCT116) were passaged at 70 to 80% confluence, washed with 1× phosphate-buffered saline (DPBS, Thermo Fisher Scientific, 14190094), and detached using TrypLE Express (Life Technologies, 12605010) - with incubation at 37 °C, 5% CO_2 for 5 min. After the cells were detached, a volume of fresh media was added to the cells (1:1 ratio of media: TrypLE) and then cells were added to the new flask with an appropriate amount of fresh media.

Protein Extraction and Quantification Protocol

Using the Eppendorf 5415R Centrifuge at RT (room temperature), 500,000 cells were harvested and pelleted at 3000*g* for 5 min. Resuspension of the cell pellet in 1 ml ice-cold DBS (Life Technologies, 14190094) and its centrifugation at RT thereafter was done for 5 min at 3000*g*. The cell pellet was re-suspended in a 1 μl protease inhibitor and a 100 μl RIPA buffer. After incubation at RT for 5 min, the supernatant collected after the lysate was centrifuged at 4 °C at 16,000*g* for 10 min. The protein in the supernatant was quantified using the Pierce BCA Protein Assay Kit (Thermo Fisher Scientific 23227) in accordance with the supplier protocol.

RNAi Knockdown

Cells were transfected according to the manufacturer (Dharmacon) protocol (Life Sciences). Cells were transfected using DharmaFect-2 (Life Sciences) with the indicated siRNA oligos (Table 1). In 6-well plates, a final concentration of 0.035 μM siRNA oligo was diluted in a 1:50 HBSS (Thermo Fisher Scientific) for each well. While the DharmaFect-2 reagent was diluted in a (2:100) HBSS, the mixture was incubated for 10 min at room temperature. A volume of 200 μl of diluted DharamFect-2 reagent was added to each well and left for 20 min at room temperature. Then fresh media was made up to a total volume of 2000 μl per well and then left for 72 h in an incubator at 37 °C, 5% CO_2.

Cellular Studies with FT671 Inhibitor

The USP7 inhibitor FT671 (MedChemExpress, HY-107985) was added to the cells at a final concertation of 10 mM for 0 h, 2 h, 4 h, 8 h, and 24 h. Cells were then trypsinized and washed once with cold PBS. For cell lysate, cells were lysed in RIPA buffer (1 ml per plate) (50 mM Tris–HCl pH8, 150 mM NaCl, 0.1% SDS, 0.5% deoxycholic acid, 1% NP-40) supplemented with protease inhibitor (Thermo Fisher Scientific) for Western blotting.

TABLE 1
List of siRNA Oligos used for transfection

Component	Code
AJUBA	MQ-021473-00-0002
siGENOME RISC-Free	D-001220-01
TRIM27	MQ-006552-01
USP7	MU-006097-01

Immunoblotting

Fifteen micrograms of protein lysate was incubated in a heating block (Benchmark) at 70 °C for 5 min with sample buffer and 0.25 M DTT and were loaded on 10% acrylamide gel and subjected to electrophoresis (120 V, 15 min then 160 V for 50 min). Using the Bio-Rad Trans-Blot Cell (Bio-Rad, 20179), proteins were transferred to a nitrocellulose membrane (GE Healthcare Life Sciences, A10224470) from the gel (4 °C, at 65 V and for 2 h) and incubated at RT for 1 h in 10 ml TBST containing 5% milk powder. Membrane was placed in its respective primary antibody solution and incubated at 4 °C overnight (Table 2). Membrane segments were then washed twice with TBST and imaged using LICOR Odyssey CLx and analyzed with Image Studio Lite V5.2 software with the scan intensity set to 4. After that, images were quantified using ImageJ with the normalization to GAPDH, actin, α-tubulin, or β-tubulin loading control to compare the density of each band.

Cell Viability

We evaluated the effect of 0.1 μl doxycycline treatment on LS88 cells during the proposed time course through CellTitre assay (Promega, 0000333156). Cells were treated using control growth media or (100 μl) growth media supplemented with 0.1 μl doxycycline and assayed at time points of 24 h, 48 h, and 72 h. Cell viability was measured using the Promega Glomax Multi detection system. Similarly, the number of cells was determined with standard column calculations and change was calculated in comparison to the cell's growth in control growth media.

Colony Formation

USP7 knockdown was performed using siRNA oligo; 2000 cells were plated in 6-well plates and the cells were incubated for 7 to 14 days. The cells were washed with PBS after the incubation and fixed with 4% paraformaldehyde (4 g paraformaldehyde + 80 ml + 20 ml of 1× PBS) for 30 min. After the fixing, the cells were washed gently with dH_2O twice and stained with 0.5% crystal violet and 20% methanol for 30 min. The cells were washed after staining with dH_2O three times and left to dry in the hood overnight before the imaging and counting took place. Colonies with at least 50 cells were counted. Each experiment was performed in triplicate.

Spheroid Assays and Quantifications

Following siRNA transfections, cells were cultured in a 96-well ultralow attachment plate (Corning-3474) in 100 μl with plating densities of 1000 (HEK 293T), 3000 (LS88 and LS174T), and 4000 (DLD-1) cells/well. Cells were cultured in 1:1 DMEM: F12, (Gibco by Life Technology) media plus 10% FBS and 1% Pen Strep (Gibco by Life Technology). The cells were incubated at 37 °C and 5% CO_2 for 14 days. Then, the images were taken using × 40 magnification. The volumes of the spheroids were calculated using the formula of volume = (4/3)πr3 using ImageJ (version1.42q). CellTiter-Glo cell viability assay was performed with the addition of 100 μl of CellTiter-Glo reagent into each well and incubated at room temperature for 1 h, followed by measurement using GloMax Discover Microplate Reader (Promega).

Immunofluorescence Microscopy

Sterile glass coverslips (22X22) were used to grow HCT116 KO USP7 cells into cell culture 6-well plates and the cells were fixed using 4% paraformaldehyde and quenched using quench formaldehyde with 10 mM glycine treatment. Cells were then permeabilized with 0.2% Triton100 and blocked 5 min at RT in 3% bovine serum albumin (BSA) blocking solution (PBS + Tween 20). Next, the slides were incubated with primary antibodies diluted in 5% BSA solution for a time period of 1 h at RT. Slides were then incubated with secondary antibodies (Alexa fluor) for 1 h 1:1000. The slides were then rinsed with BSA solution then with PBS. Coverslips were mounted overnight with the help of ProLong Gold antifade mounted with DAPI. A Leica TCS SP8 microscope was then made use of to visualize the slides; this was acquired using LAS X Core software (V3.3.0). For the subcellular analysis of LS88, cells were untreated/treated with doxycycline. Fiji (ImageJ) was used to create regions of interest for the measurement of image mean gray value for cytoplasm, nucleus, and local background (n = 20). Data were corrected by subtracting local background values from cytoplasm and nucleus mean gray values. Mean, SD, and *t* test *p*-value were calculated, and intensity data was expressed as percentage of control values.

TABLE 2
Details of primary and secondary antibodies used in Western blot

Antibody	Company	Product code	Host species	Dilution
Primary Antibodies				
AJUBA	Santa Cruz Biotechnology	sc-374610	Mouse	1:1000
Alpha-Catenin	Cell Signaling	3240	Rabbit	1:1000
Alpha-Tubulin	Cell signaling	2144S	Rabbit	1:1000
DSG2	Antibodies	A101469	Rabbit	1:1000
E-Cadherin	Cell signaling	3195	Rabbit	1:1000
Integrin beta4	Antibodies	A94529	Rabbit	1:1000
ITGA6	Antibodies	A9166	Rabbit	1:1000
Jup	Cell Signaling	75550S	Rabbit	1:1000
N-Cadherin	Cell signaling	D4R1H	Rabbit	1:1000
P53	Santa Cruz Biotechnology	DO-1:SC-126	Mouse	1:1000
USP7	Santa Cruz Biotechnology	H200 sc-30164	Rabbit	1:1000
USP7 (For COIP)	Santa Cruz Biotechnology	(H-12) sc-137008	Mouse	1:1000
Secondary Antibodies				
Rabbit 680CW	LI-COR	925-68021	Goat	1:10,000
Rabbit 800CW	LI-COR	925-32211	Goat	1:10,000
Mouse 680CW	LI-COR	925-68020	Goat	1:10,000

Immunoprecipitation

The cells were lysed for 30 min at 4 °C in pNAS buffer (50 mM Tris/HCl (pH 7.5), 120 mM NaCl, 1 mM EDTA, and 0.1% Nonidet P-40) with protease inhibitors. Cells were scratched and kept on ice for 30 min, and then proteins were quantified using bicinchoninic acid assay. For input, 40 μg of samples were aliquoted. Protein G Sepharose beads were utilized after washing them with 1× PBS three times. The concentration of immunoglobulin G (IgG) agarose and the antibody samples were 1 mg/ml. In addition, 40 μl of the shacked beads were added to the IgG and antibody samples and rotated for 1 hr. Next, the IgG agarose and antibody samples were spun down in the centrifuge (570*g* at 4 °C) for 1 min. In a new Eppendorf, 950 μl from the supernatant was taken. Subsequently, 50 μl of the Protein G Sepharose beads were added to the antibody samples and IgG. Indicated antibodies and IgG were added to the lysate for 16 h at 4 °C. The samples and IgG were spun down (570*g* at 4 °C for 1 min). Immunoprecipitates were washed four times with cold PBS followed by the addition of SDS sample buffer. The bound proteins were separated on SDS polyacrylamide gels and subjected to immunoblotting with the indicated antibodies.

RNA Extraction

RNeasy Mini Kit (Qiagen) was used to extract RNA from the samples according to the manufacturer's protocol. Cells plated in a 6-well plate were washed with 1× PBS twice after the media was removed. The cells were lysed with 350 μl of buffer RLT in each well. After pipetting several times, 350 μl of 70% ethanol were added into the lysate and mixed well. Seven hundred microliters of mixture was then transferred into each RNeasy Mini spin column and centrifuged at maximum speed for 30 s. After discarding the flow-through, 500 μl of buffer RW1 was added onto the spin column and centrifuged, following two steps using 500 μl of the buffer RPE and centrifuged at maximum speed for 30 s and 2 min. Finally, 40 μl of RNase-free water was added to RNeasy spin column which was placed in a new 1.5 ml Eppendorf and centrifuged at maximum speed for 1 min. To quantify RNA concentration, a Nanodrop Spectrophotometer 2000c, (Thermo Fisher Scientific) was conducted. And the RNA samples were stored at –80 °C until qPCR was performed.

Quantitative Real-Time PCR

RNA samples with a final concentration of 20 ng/μl were diluted in RNase free water (Qiagen) and used in this experiment. A QuantiNova SYBR Green RT-PCR kit (Qiagen) was utilized to perform real-time PCR according to the manufacturer's instructions. The reaction set-up (Table 3), the primers (FW-USP7 - 5′- GGA CAT GGA TGA CAC CA -3′), (RV-USP7- 5′- TCA CTC AGT CTG AAG CG -3′), (FW-AJUBA- 5′- GAG AAC CCT CGG GGA TTG A -3′), and (RV-AJUBA- 5′- GCA CTT GAT ACA GGT GCC GAA -3′) (Integrated DNA Technologies), and the thermocycling conditions were listed (Table 4).

TABLE 3
qRT-PCR reaction set-up using a QuantiNova SYBR Green RT-PCR kit (Qiagen)

Name of component	Volume(μl)
RNA (20 ng/μl)	1
Gene-specific primer(20×)	1
2× Rotor-Gene SYBR Green PCR Master Mix ROX reference dye	10
SYBR Green RT Mix	1
RNase-free H2O	0.2
	Add to 20 μl

TABLE 4
Thermocycling conditions for qRT-PCR (StepOnePlus, Thermo Fisher Scientific)

Condition	Temperature	Time	Cycles
RT-step	50 °C	10 min	40
PCR initial heat activation	95 °C		
Denaturation	95 °C	5 s	
Combined annealing and extension	60 °C	10 s	
Melt Curve stage			
Denaturation	95 °C	15 s	
Annealing	60 °C	1 min	
High resolution melting	95 °C	15 s	

Work on each sample was performed in triplicate in a 96-well plate on a StepOnePlusTM Real-Time PCR System (Thermo Fisher Scientific). The fluorescent dye was released during amplification. The point at which the intensity exceeded the threshold was recorded in order to determine the Ct value. The more significant the Ct value, the later the intensity exceeded the threshold, and the lower the expression of that specific gene. Gene expression of each sample was evaluated from the ΔΔCt value utilizing ACTB (β-Actin) as a control. The results were analyzed in GraphPad Prism, version 9.3.1 (GraphPad Software Inc).

Dispase Mechanical Stress Assay

Intercellular adhesion was evaluated by incubation with the dispase enzyme on cell monolayers followed by a mechanical stress test, then the cell monolayers were assessed using light microscopy. LS88, control siRNA, and USP7- or Ajuba-depleted cells were seeded in 6-cell culture plates (Corning) with three replicates for each condition and grown until reaching confluency. The cell monolayers were washed with Hanks' Balanced Salt Solution (HBSS) (14025092, Thermo Fisher Scientific) after the media was removed from the cultures. The cell monolayers were incubated with dispase enzyme (2.5 units/ml in HBSS) (D4693, Sigma) at 37 °C for 30 min or longer in order to detach the monolayers from the plate bottom. Once the monolayers detached, they were imaged using a Leica M2 16 F microscope and S Viewer V3.0.0 software. After that, the monolayers were subjected to mechanical stress by pipetting with 1 ml HBSS and shaking in the shaker for 3 min at 300 rpm. The fragments were counted for all three conditions and imaged.

Experimental Design and Statistical Rationale

This study compares the proteomes of LS88 cells with USP7 inducibly knocked-down using doxycycline to control cells with WT levels of USP7. We analyzed 9 mass spectrometry (MS) samples in total consisting of three groups with three biological replicates in each group (1) LS88 untreated at 0 h, (2) LS88 untreated at 72 h, and (3) LS88 treated with doxycycline at 72 h. These treatments were based upon results presented in Figure 1 and in the Supplementary Data, and we observed good correlation between biological replicates based upon the principal component analysis (PCA) and unsupervised clustering shown in Figure 2. To identify proteins that are significantly decreased following treatment with doxycycline and USP7 knockdown, we compared the LS88 cells untreated (at 72 h) with LS88 cells treated with doxycycline (at 72 h). Only proteins identified with peptides across all six of these samples were considered when performing the comparisons. For all analysis of Western blot densitometry, paired or unpaired Student's t-tests were performed as appropriate in GraphPad Prism 9.2 software. For all statistical

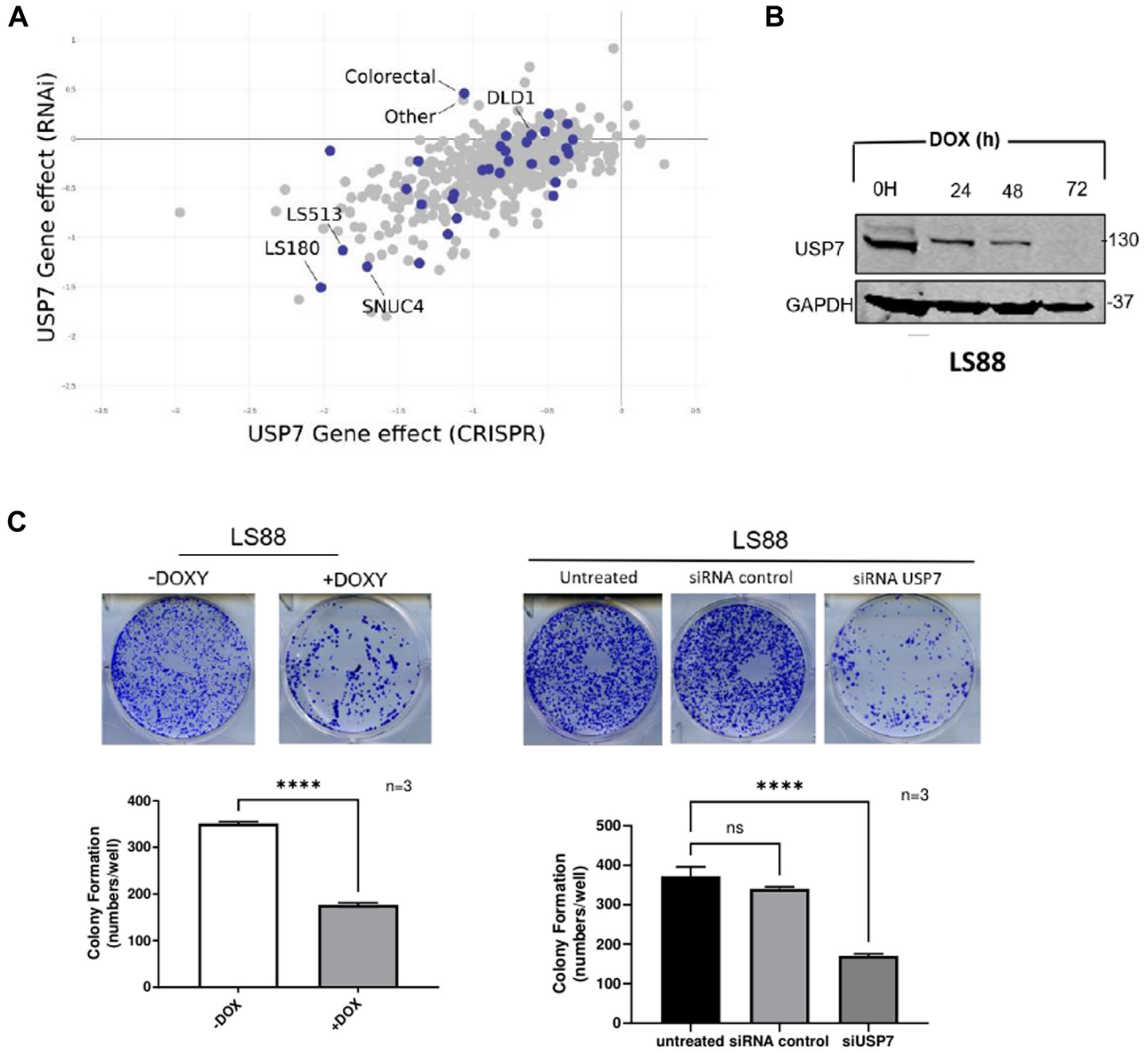

FIG. 1. **LS180 is an effective model for investigating USP7 function in colorectal cancer.** *A*, scatterplot comparing the distribution of USP7 gene effect processed scores (CERES, DEMETER2) between the RNAi dataset (y) and CRISPR dataset (x). Selected cell-lines with the largest USP7 gene-effect scores from RNAi and CRISPR are labeled in addition to DLD1, an additional CRC cell-line used in this study. All analysis performed in DepMap portal (depmap.org). *B*, efficient degradation of USP7 at the indicated time points. LS88 colon carcinoma cells stably carrying a pTER-USP7 shRNA construct and a Tet repressor (TR)-construct were treated with 1 μg/ml doxycycline for 24, 48, and 72 h and examined by Western blotting for reduction of endogenous USP7; GAPDH was used as a loading control. *C*, LS88 cells (with inducible siRNA targeting USP7) were treated with 1 μg/ml concentrations of doxycycline for 72 h before being seeded in 6-well plates and incubated for 7 to 14 days. Graph represents mean ± SD (two tailed, unpaired *t* test), $p \leq 0.0001$.

comparisons of more than two groups, ordinary one-way ANOVA was conducted with GraphPad Prism 9.2 software.

Proteomic Sample Preparation and MS

Lysis of the protein pellets (0.1 M TEAB, 0.1% SDS) was performed with pulsed sonication and then samples were centrifuged (up to 10 min, 13,000*g*). The extraction of methanol/chloroform was done on 40 μg of protein for each lysate and finally, the pellets were re-dissolved in 100 μl of 6 M Urea (Sigma), 2 M thiourea (Sigma), 10 mM Hepes buffer (Sigma), pH = 7.5. This was followed by the reduction of the samples (1M DTT), alkylation (5.5 M iodoacetamide), and then dilution in 400 μl of 20 mM ammonium bicarbonate (Sigma) and digestion with trypsin (Promega) (1/50 w/w) overnight. Acidification of each sample (pH < 3.0) was done with the TFA (Sigma) and solid phase extraction performed using waters oasis HLB prime μElution 96-well solid phase extraction plate. Plate collection vessel was used in the plate vacuum manifold and the plate was conditioned

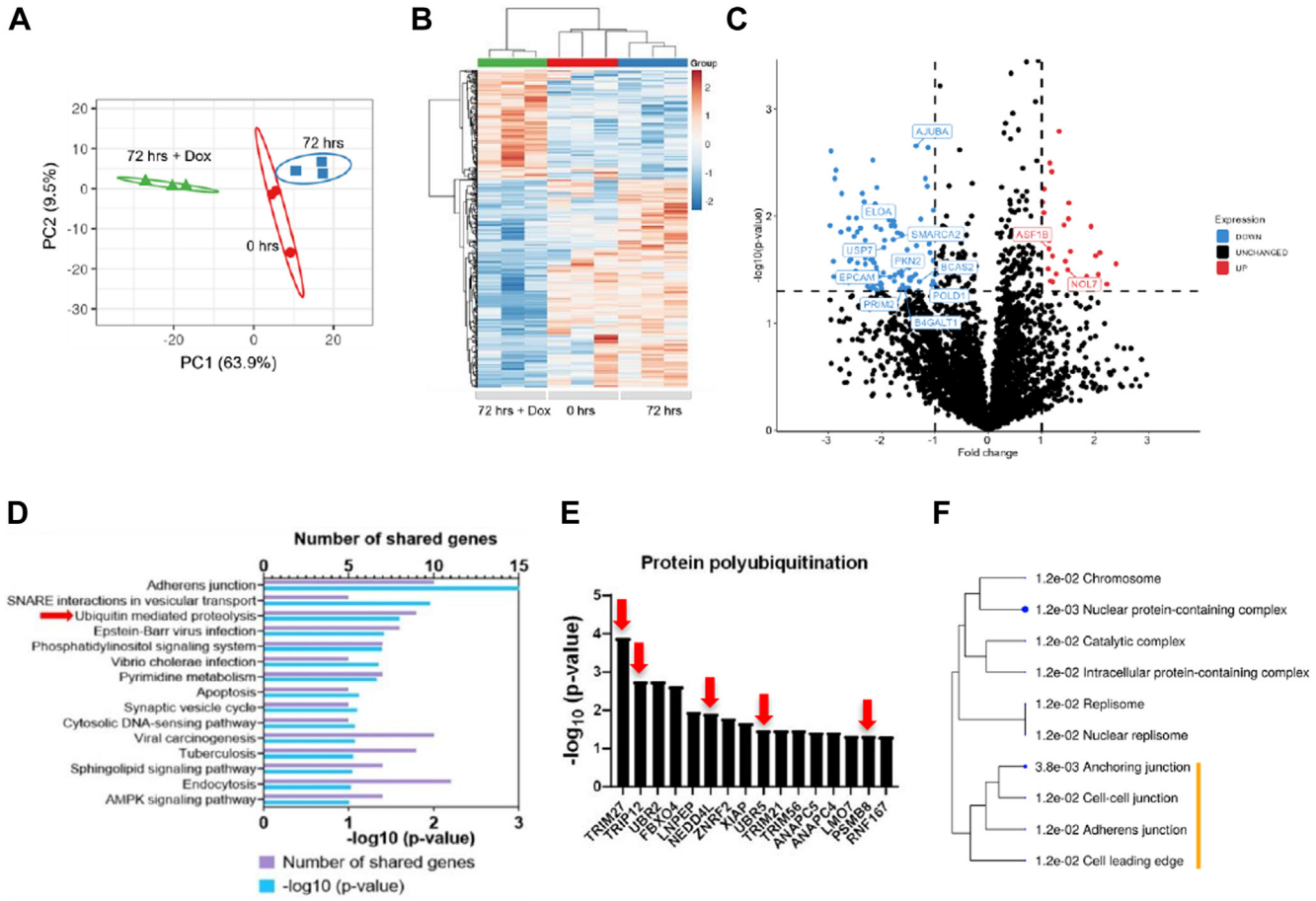

FIG. 2. **Proteomic analysis of LS88 with/without doxycycline treatment for USP7 knockdown.** *A*, principal component analysis scores plot showing the clustering of proteins according to their distributions in different groups. Control LS88 represents cells at hour zero (0 h), LS88 treated with doxycycline for 72 h (72 h + doxycycline) or left without treatment for 72 h (72 h). *B*, heatmap of normalized intensity values (light/low – dark/high) for each group (0 h untreated; 72 h untreated; 72 h + doxycycline). All proteins (N = 444) with $p < 0.05$ for treated *versus* untreated (at 72 h) are included. *C*, volcano plot showing differentially responsive proteins in comparison of 72 h untreated *versus* 72 h doxycycline-treated cells. Selected proteins from enriched pathway and process categories are labeled. *D*, annotation analysis of the sets of proteins ($p < 0.05$) decreased following doxycycline treatment (after 72 h). Pathways from DAVID tool are sorted by *p* value and the top 15 most significantly enriched pathways shown. Ubiquitin-mediated proteolysis category is indicated by arrow. *E*, the top 15 most significantly decreased proteins ($p < 0.05$) following doxycycline treatment (after 72 h) that are involved in protein polyubiquitination. TRIM27, a USP7 protein-complex partner, is the most significantly altered protein following USP7 knockdown in this category (Analysis performed in Metascape). Proteins that are known to be direct substrates or interaction partners of USP7 (according to STRING) are indicated with arrow. *F*, dendrogram showing significant Gene Ontology cellular components for the set of proteins ($p < 0.05$) decreased following doxycycline treatment. Enrichment *p*-values are indicated and only GO terms with FDR *p*-value <0.05 were included. GO terms associated with cell-cell junction functions are highlighted with *orange* bar. Dendrogram circle shape size indicates *p*-value.

with the addition of 200 µl of acetonitrile. The wells were equilibrated through 200 µl of 0.1% TFA and then inserting a 96-well collection plate. There was a further application of 100 µl of sample to each well and of a low vacuum. A protective cover was used to cover the 96-well collection plate and was stored at 4 °C. The collection plate was replaced with the vessel again. The wells were washed using 2 × 700 µl of 0.1% TFA and then 200 µl of water in order to remove buffer and salts. Addition of 70% of acetonitrile to the well was done to evaporate the remaining liquid followed by re-suspension in buffer A (H_2O + 0.1% Formic Acid). To meet the internal quantification standard, 200 fmol of Waters enolase (*Saccharomyces cerevisiae*) standard were further added to each of the samples.

Peptide extracts (1 µg on column) were separated on an Ultimate 3000 RSLC nano system (Thermo Fisher Scientific) using a PepMap C18 EASY-Spray LC column, 2 µm particle size, 75 µm × 75 cm column (Thermo Fisher Scientific) over a 140 min (single run) linear gradient of 3 to 25% buffer B (0.1% formic acid in acetonitrile (v/v)) in buffer A (0.1% formic acid in water (v/v)) at a flow rate of 300 nl/min. Peptides were introduced using an EASY-Spray source at 2000 V to a Fusion Tribrid Orbitrap mass spectrometer (Thermo Fisher Scientific). The ion transfer tube temperature was set to 275 °C. Full scans were acquired in the Orbitrap analyser using the Top Speed data dependent mode, performing a MS scan every 3 s cycle, followed by higher energy collision-induced dissociation MS/MS scans. MS spectra were acquired at a resolution of 120,000 at 300 m/z, RF lens 60%, and an automatic gain control ion target value of 4.0e5 for a maximum of 100 ms. Peptide ions were isolated using an isolation width of 1.6 amu and trapped at a maximal injection time of 120 ms with an automatic

gain control target of 300,000. Higher-energy collisional dissociation fragmentation was induced at an energy setting of 28 for peptides with a charge state of 2 to 4. Fragments were analyzed in the orbitrap at 30,000 resolution.

Mass Spectrometry Data Processing and Analyses

Analysis of raw data was performed using (1) Proteome Discoverer software (Thermo Fisher Scientific) (version 2.4) and (2) Mascot search engine (version 2.7.0.1). For (1) the data was processed to generate reduced charge state and deisotoped precursor and associated product ion peak lists. These peak lists were searched against the Human UniProt protein database (080620) (570,420 protein sequences). A maximum of one missed cleavage was allowed for tryptic digestion and the variable modification was set to contain oxidation of methionine and N-terminal protein acetylation. Carboxyamidomethylation of cysteine was set as a fixed modification. The false discovery rate (FDR) was estimated with randomized decoy database searches and were filtered to 1% FDR. Mass tolerance for precursor ions was set at ± 1.2 Da and for fragment ions at ± 0.6 Da.

For Mascot searches, peak lists were generated using ProteoWizard's msconvert (version 3.0.23213) to convert the raw peak .RAW files into .mgf peak lists for Mascot (2023 release). Thereafter, the .mgf files searched using Mascot server using its default parameters against UniProt's *Homo sapiens* proteome (UniProt proteome ID UP000005640) and Proteomics Identifications Database (PRIDE) contaminants spectra (Release: 2015-04-01, Version: 2015-04). The FDR threshold was set at 0.05. Trypsin (X-[K/R]) was used for the digestion with two allowable missed cleavages. The variable modifications used in the search included the following: oxidation of methionine and carbamidomethylating of cysteine. No fixed modifications were included in the search. Mass tolerance for precursor ions was set at ± 1.2 Da and for fragment ions at ± 0.6 Da. Identified proteins were filtered by setting a FDR threshold of 1%.

The mass spectrometry data has been submitted to the PRIDE database with the following details:

Project accession: PXD039488
Project DOI: 10.6019/PXD039488
Reviewer account details:
Username: reviewer_pxd039488@ebi.ac.uk
Password: ReyeLEaT

Additional Bioinformatics Analyses

For the analysis of vulnerabilities across cancer cell lines, the Cancer Dependency Map (21) CRISPR and RNAi data were used (version Public 24Q2). All analysis and plots were generated through the DepMap portal (https://depmap.org/portal). To investigate pathways and gene enrichment in the MS proteomics data, the set of 445 proteins which were significantly ($p < 0.05$) altered between the doxycycline-treated LS88 cells and the untreated LS88 cells at 72 h were analyzed. Several tools were used: the (DAVID) functional annotation web tool (version 6.8; https://david.ncifcrf.gov) (22), the ShinyGO interface and tool (23) (default settings, FDR cutoff = 0.05), and Metascape pathways analysis tool (24) (default settings).

RESULTS

Selection and Optimization of a Cell Model for Analysis of USP7 Function in CRC

To identify a suitable cell model for the analysis of USP7 function in CRC, we first analyzed publicly available cancer-dependency profiles from the DepMap project (21). The DepMap project includes both large-scale CRISPR and RNAi screens of many cancer cell-lines and provides a significant resource for identifying the vulnerabilities of different cancer types using knockout or knockdown screens. We analyzed the CRISPR and RNAi dependency scores across all cell-lines in the DepMap as shown in Figure 1*A* and noted that several CRC cell-lines show strong negative gene-effect scores in both the CRISPR and RNAi datasets. Notably, growth of the LS180 cell-line is significantly inhibited through either USP7 knockdown or knockout in the DepMap project (Fig. 1*A*). LS180 is a human colon adenocarcinoma cell line derived from a 58-year-old Caucasian female with Dukes type B adenocarcinoma of the colon (ECACC 87021202). The related LS174T cell line (ECACC 87060401) was derived from the same patient ("ECACC General Cell Collection: 87021202 LS180," n.d.) and were subsequently modified to express a doxycycline-inducible siRNA construct pTER-USP7 (cell-line known as LS88) (20). We used this LS88 cell-line as the basis of our proteomic screen in this study. To identify suitable conditions for the proteomic screen, we confirmed that treatment of LS88 cells with doxycycline-induced knockdown of USP7 in a time-dependent manner (Fig. 1*B*) and that levels of Trim27 and p53, two key proteins regulated by USP7, were regulated as expected according to previous studies (25) following doxycycline treatment (Supplemental Fig. S2). We next showed that cell viability is significantly affected following treatment of LS88 cells with doxycycline- or siRNA-induced knockdown of USP7 (Fig. 1C). Further results of cell viability and colony formation following USP7 knockdown are provided in Supplemental Fig. S1. We also confirmed that the observed decreases in cell viability were due to USP7 knockdown and not treatment with doxycycline per se, since doxycycline is known to have a negative effect on invasive potential and cell proliferation across varied human CRC cell lines (26, 27) (Supplemental Fig. S3). Finally, we also showed that inducible knockdown for 72 h in LS88 cells with doxycycline has similar effects to USP7 depletion *via* siRNA in another CRC cell-line, DLD-1. Notably, the DLD-1 cell-line, in common with many other CRC cell-lines, has mutant-truncated APC, and a previous study indicated that USP7 has a specific role in maintaining Wnt signaling in tumors with APC mutations (28). We also observed that in the DepMap (depmap.org) gene-effect data, the effect of USP7 knockout or knockdown is markedly less pronounced in CRC cell-lines with APC mutation than in those without (Supplemental Fig. S4). In summary, the USP7 inducible knockdown cell-line LS88 in the highly USP7-dependent CRC cell line of LS180 represent an appropriate model for studying USP7 function in CRC. The effects are comparable to other widely used CRC cell-lines following USP7 depletion.

Analysis of the USP7 Network Using Inducible Knockdown Proteomics

To broadly characterize proteome-wide altered protein expression in response to USP7 knockdown, we performed whole-cell profiling using quantitative label-free LC-MS/MS. Based on the altered phenotypic properties of the doxycycline-treated LS88 cells observed above, we compared doxycycline-treated LS88 cells at 72 h to control (untreated) cells at 0 and 72 h after the start of the experiment. Three replicate samples were profiled using LC-MS/MS for each group. Data-dependent quantitative MS analysis identified a total of 7301 proteins of which 445 proteins were found to be significantly ($p < 0.05$) differential between the treated and untreated samples at 72 h. We then analyzed the data and sample reproducibility as shown in Figure 2, *A–C*. The PCA and unsupervised clustering analyses (Fig. 2, *A* and *B*) showed that intra-group variability was low in comparison to that between groups and that the doxycycline-treated cells have quite distinct expression profiles from the untreated cells at 0 and 72 h. We therefore visualized the proteins and their differential abundance between doxycycline-treated and untreated samples in the volcano plot shown in Figure 2*C*. This showed a significant set of both increased and decreased proteins following doxycycline treatment. As expected, USP7 itself is one of the most significantly decreased proteins. In addition, the Ajuba protein (labeled) showed significant decreased abundance in doxycycline-treated cells. Since our goal is to identify proteins whose expression decreases alongside depletion of USP7 (and are therefore potential substrates of the USP7 deubiquitinase), we analyzed the set of 293 proteins which were significantly ($p < 0.05$) decreased following doxycycline treatment. We first analyzed these proteins using DAVID (22) to broadly assess the most significant pathways (Fig. 2*D*). We noted that proteins related to ubiquitination-mediated proteolysis represent a significantly enriched group and show this set of proteins in Figure 2*E*. Notably, the top two proteins, TRIM27 and TRIP12 are known interaction partners of USP7 (29, 30), suggesting that our dataset could be a rich source of USP7 substrates and novel interaction partners. We also noted that from the DAVID analysis, adherens junctions proteins represent the most significantly enriched group within the data. We further analyzed this finding using ShinyGo (23) to represent the 10 most significant GO cellular components as shown in Figure 2*F*. Although USP7 has been implicated in the regulation of several cancer-associated pathways, its role in the regulation of cell-cell adhesion is relatively unstudied. We focused on the Ajuba protein that was previously found to promote growth, migration, and metastasis in CRC, in addition to its roles and functions in regulating cell-cell adhesion and pathways such as Hippo (31). The volcano plot (Fig. 2*C*) is annotated with key proteins from this study and with selected proteins from the most significant GO cellular component categories in Figure 2*F*. Finally, protein intensity values are provided for those proteins analyzed by Western blot in Supplemental Fig, S5.

USP7 Sustains Ajuba Protein Stability in CRC Cells

Ajuba was significantly decreased in response to doxycycline in the MS proteomic analysis (Fig. 2*C*), and we first confirmed this response using immunoblotting. The level of Ajuba protein after USP7 inhibition was determined at different time points (0, 24, and 72 h) using doxycycline (1 μg/ml) in LS88. We observed a reduction of Ajuba expression after USP7 depletion and a particularly marked decrease in Ajuba after 72 h following doxycycline treatment, comparable to the time point used in the MS proteomics study (Fig. 3, *A* and *B*). We further explored this effect by using FT671, a noncovalent selective USP7 inhibitor. We treated LS88 cells with the FT671-USP7 and the levels of Ajuba was analyzed using Western blot (Fig. 3*C*). As shown in the Figure, we did observe some decrease of the Ajuba protein levels after 48, 72, and 96 h following treatment. Similarly, the results from a different CRC cell line (HCT116) showed a reduction of Ajuba protein expression after the cells were treated with the inhibitor for 48 and 72 h (Fig. 3*D*). We therefore confirmed that the doxycycline-induced decrease of Ajuba in the LS88 cells resembles the response seen in CRC cells treated with a selective USP7 inhibitor, suggesting that Ajuba is dependent on USP7 for its stability and abundance.

We then analyzed the subcellular localization of Ajuba and USP7 using immunofluorescence. As shown in (Fig. 4, *A–C*) Ajuba and USP7, protein levels were markedly decreased in LS88 cells treated with doxycycline (1 μg/ml) where USP7 was downregulated. Ajuba was previously reported to localize mainly in the nucleoplasm and the Golgi apparatus (32), and USP7 was reported to localize predominantly to the nucleus (33). In concordance with this finding, we observed that Ajuba and USP7 protein levels were very significantly ($p < 0.0001$) higher in nuclei than in cytoplasm ($p < 0.001$) in the cells treated with doxycycline which is consistent with their localization (Fig. 4*C*).

USP7 Regulates Ajuba at the Posttranslational Level

In order to further investigate the regulatory relationship between Ajuba and USP7, we used qRT-PCR to show that Ajuba mRNA expression was unaffected by USP7 downregulation in doxycycline-treated LS88 cells (Fig. 5, *A* and *B*), showing that USP7 does not regulate Ajuba at the transcriptional level. We next investigated whether Ajuba is

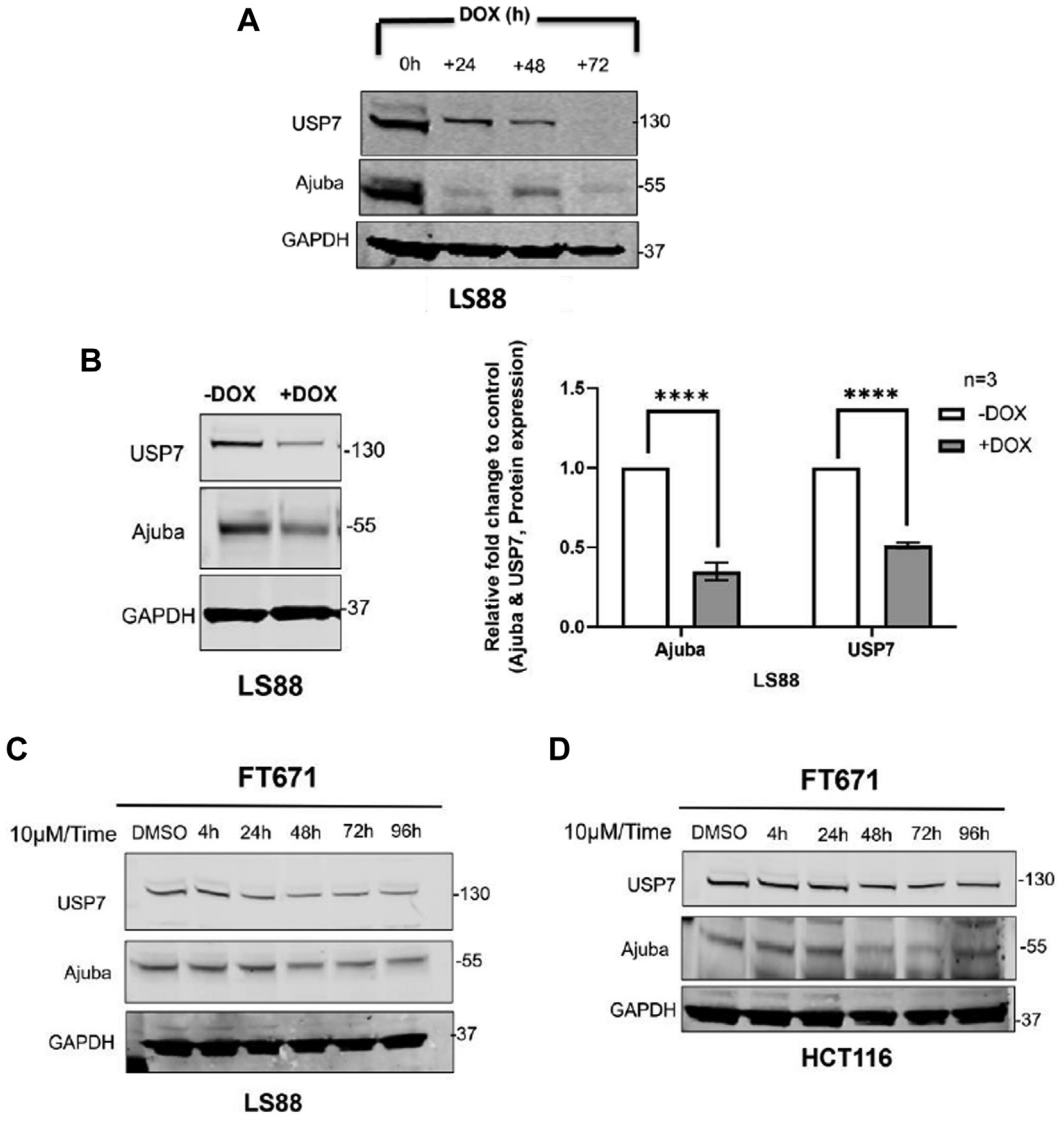

FIG. 3. **Western blot analysis of Ajuba abundance following USP7 knockdown.** *A*, total cell lysate treated with doxycycline in different time point were collected and analysis using immunoblotting. *B*, LS88 cells treated or untreated with doxycycline were examined on Ajuba protein expression. Unpaired Student's *t* test was used for three independent experiments. $p < 0.0001$. GAPDH was used as a loading control. *C*, total cell lysates from LS88 and (D) HCT116 treated with FT671 (10 μM) for indicated times. GAPDH is a loading control.

a protein–protein interaction partner of USP7 by using immunoprecipitation with anti-USP7 antibodies in LS88 cells. We found that USP7 interacts with Ajuba in CRC cells when USP7 is pulled down and analyzed by immunoblotting (Fig. 5*C*), showing that Ajuba is indeed a physically associated interaction partner of USP7 in CRC. We also found in both LS88 and LS147T cells that reciprocal knockdown of Ajuba does not alter USP7 protein levels (Fig. 5*D*), indicating that USP7 and Ajuba are not co-complexed proteins with mutual regulation of protein stability but rather that Ajuba protein stability is dependent on USP7 but not vice-versa.

Knockdown of USP7 or Ajuba Causes Disruption of Cell-Cell Adhesion in CRC Cells

Since cell-cell and adherens junctions were found to be one of the most significantly enriched functions from the proteomic analysis (Fig. 2), we analyzed whether knockdown of USP7 or Ajuba resulted in phenotypic changes to cell-cell adhesion. Dispase assays allow for the separation of cell culture monolayers that can then be subjected to mechanical stress. As shown in Figure 6, mechanical stress of siUSP7- or siAJUBA-treated cells led to significantly increased fragmentation of monolayers as compared to control siRNA treatments, showing that reduction of either USP7 or Ajuba causes

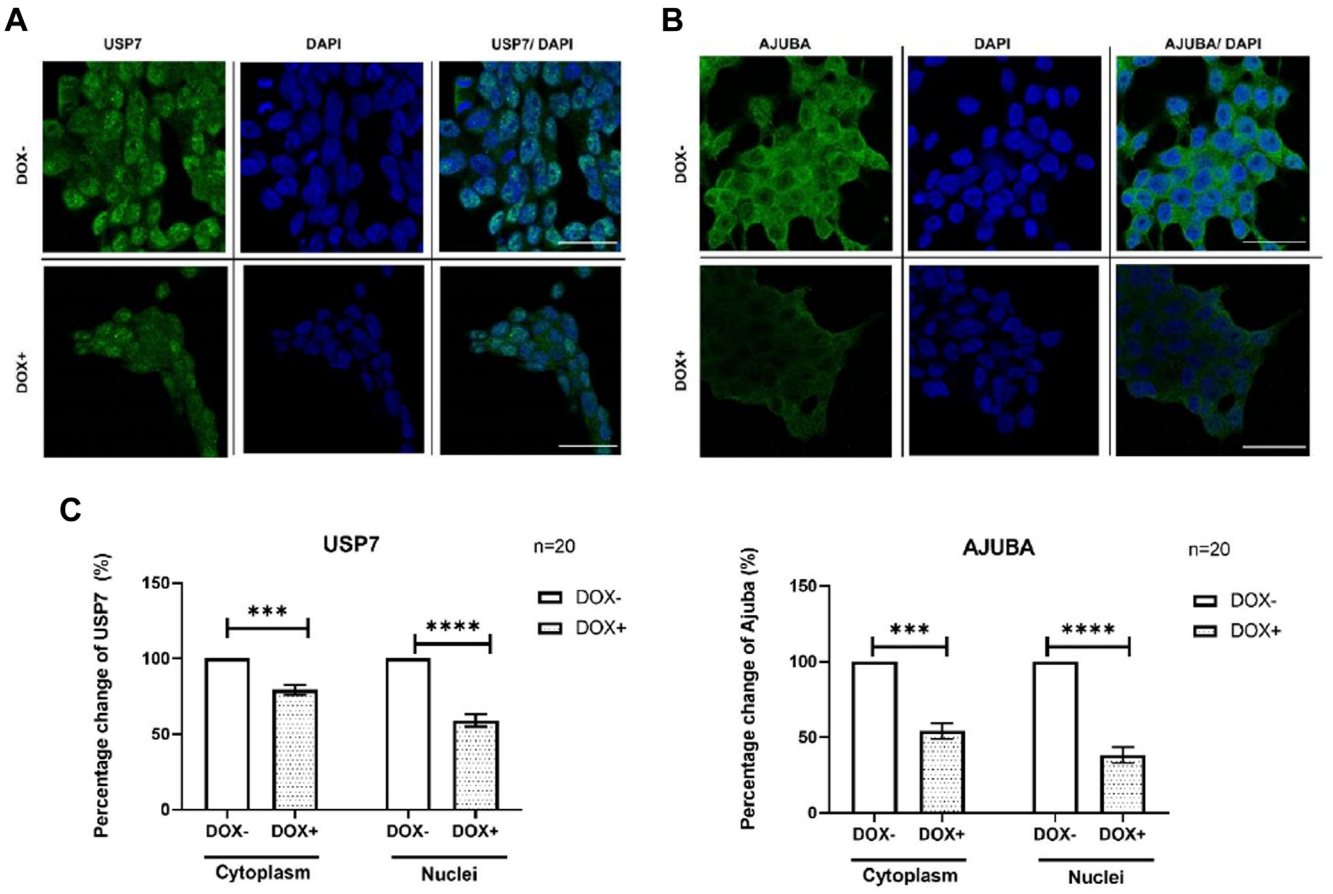

FIG. 4. **Immunofluorescence analysis of Ajuba levels following USP7 knockdown in LS88 cells.** *A*, immunofluorescence staining of Ajuba, (B) USP7 (*green*) in LS88 cells treated with doxycycline (DOX+) or untreated (DOX–). Cells were fixed and stained with DAPI (*blue*) to stain nuclei. Scale bars represents 30 μm. *C*, data were corrected by subtracting local background values from cytoplasm and nucleus mean *gray* values. Statistical differences were determined by Unpaired *t* test of percentage change of Ajuba and USP7 in cytoplasm and nuclei in LS88 cells. Data are mean ± SD.

a very significant reduction in the mechanical strength of cell-cell adhesion in CRC cells.

Knockdown of USP7 or Ajuba Disrupts Cadherin but Not Catenin Protein Levels

To identify the underlying mechanisms of how cell-cell adhesion is disrupted through USP7 or Ajuba knockdown, we examined the expression of cell junction–associated proteins. Since Ajuba has been identified to interact with several cadherins and catenins (CDH1/E-cadherin, CTNNA1/α-catenin, CTNNB1/β-catenin, CTNND1/δ-catenin, and JUP/plakoglobin), we focused our analysis on this group of proteins. Using immunoblotting, we investigated the protein levels of multiple cadherins and catenins following USP7 or Ajuba knockdown. As shown in Figure 7*A*, both N-cadherin and E-cadherin protein levels were reduced after USP7 inhibition in LS88 cells, and similarly, the expression of N-cadherin and E-cadherin were reduced following USP7 knockdown in HCT116 cells (Fig. 7*B*). We also observed that treatment of LS88 and HCT116 cells with the USP7-inhibitor FT671 across a time course resulted in decreased N-cadherin expression (Supplemental Fig. S6). Since these findings suggest that USP7 may regulate cadherin expression in CRC cells, we employed IP-coupled westerns (co-IP) to determine whether there is a physical interaction between USP7 and E-cadherin. This analysis (Fig. 7*D*) did not indicate that there was a physical interaction between the proteins, suggesting that, at least under the conditions used, the reduction in E-cadherin expression is not mediated *via* interaction with USP7 and that E-cadherin is not a substrate of the deubiquitinase. Although USP7 has been shown to regulate Wnt/β-catenin signaling in CRC (28, 34, 35), we found no altered β-catenin protein expression following USP7 knockdown in multiple CRC cell-lines (Supplemental Fig. S7), except in SW480 cells, that carry the APC truncation mutation which results in β-catenin stabilization, in line with a previous publication (34). Similarly, there was no effect on either α-catenin or JUP/plakoglobin following USP7 knockdown (Fig. 7*C*). We observed that levels

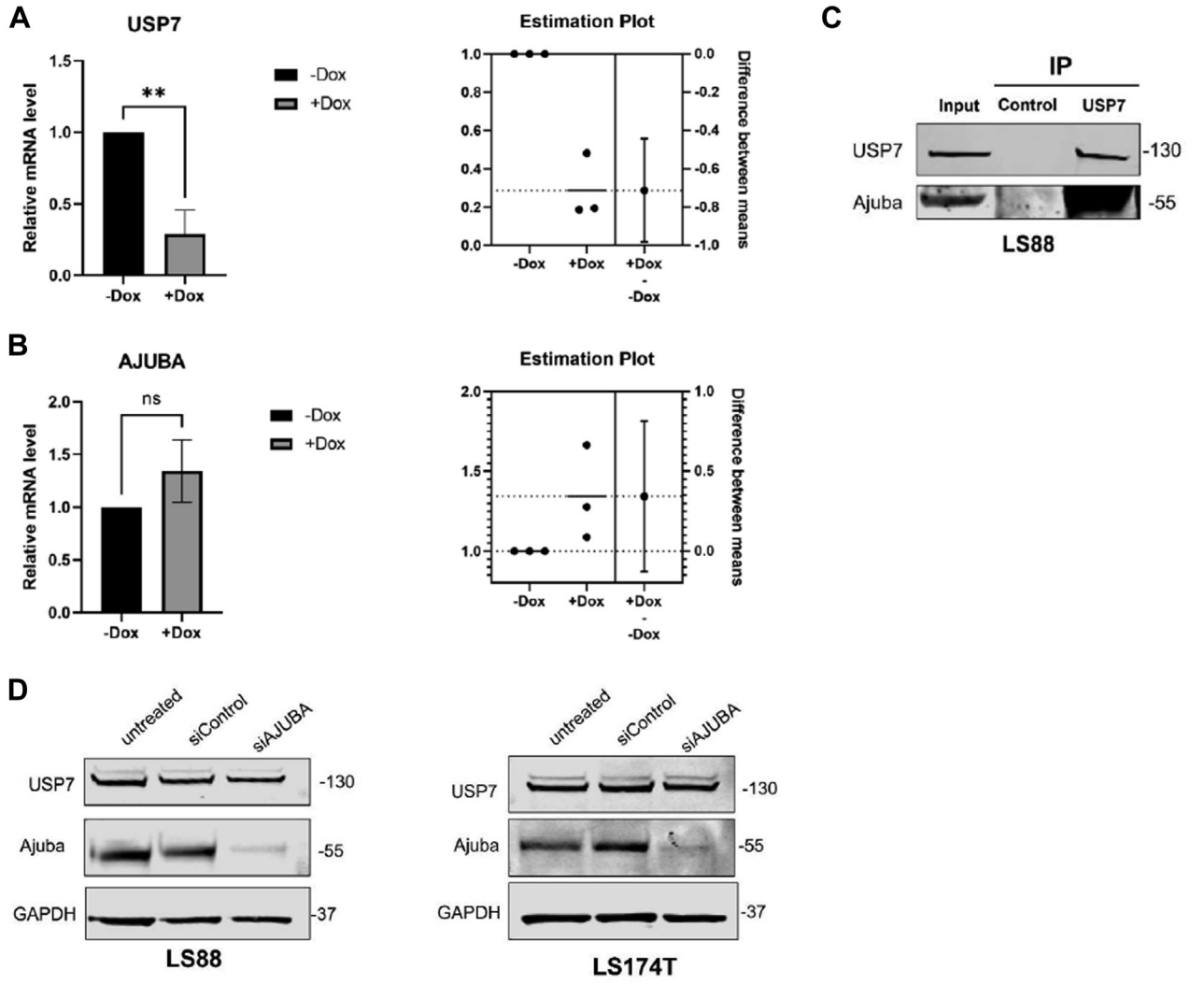

FIG. 5. **USP7 interacts with Ajuba and Ajuba knockdown does not affect USP7 protein levels in CRC cells.** *A*, mRNA levels of USP7 in doxycycline-treated (DOX+) or untreated (DOX-) LS88 cells. $^{**}p < 0.01$. Data are mean ± SD. *B*, mRNA levels of Ajuba in DOX + or DOX- LS88 cells. Unpaired t-tests were used for analysis in order to assess any differences between the means. Experiments were performed in triplicate, n = 3. *C*, LS88 cells total lysates were immunoprecipitated with anti USP7 antibody or IgG, and Ajuba was analyzed using indicated antibodies in LS88 cells. *D*, LS88 and LS174T cells expressing Ajuba, control siRNA, or Ajuba siRNA were analyzed by Western blotting and USP7 protein expression were examined using the indicated antibodies. As a loading control, GAPDH protein levels were assessed.

of JUP were increased ($p < 0.05$) following USP7 depletion in the proteomics data but did not observe any increase using Western blots nor was there an interaction detected *via* co-IP (Fig. 7*D*).

Since Ajuba knockdown resulted in loss of cell-cell adhesion similarly to USP7 (Fig. 6*B*), we next examined the expression of cell junction–associated proteins in response to Ajuba knockdown. Since desmosomes and hemidesmosomes play key roles in cell-to-cell adhesion and cell-basement membrane adhesion (36), we investigated the hemidesmosome protein integrin alpha 6 (ITGA6), the hemidesmosome protein integrin subunit beta 4 (ITGB4), and desmosomes protein Desmoglein-2 (DSG2) in doxycycline-treated LS88 cells and Ajuba knockdown cells. We observed a marked decrease in the expression of ITGB4 protein in Ajuba-inhibited cells (Fig. 8, *A*–*C*), but no other detectable changes were observed.

Next, LS88 cells were left untreated or transfected with siControl or siAJUBA, and a Western blot was performed to examine JUP. We found a measurable decrease in JUP abundance in LS88 cells (Fig. 8, *D* and *E*); however, no significant change was detected in JUP abundance in AJUBA-depleted cells in LS174T (Fig. 8*F*). We also examined α-catenin and N-cadherin protein levels in LS88. The

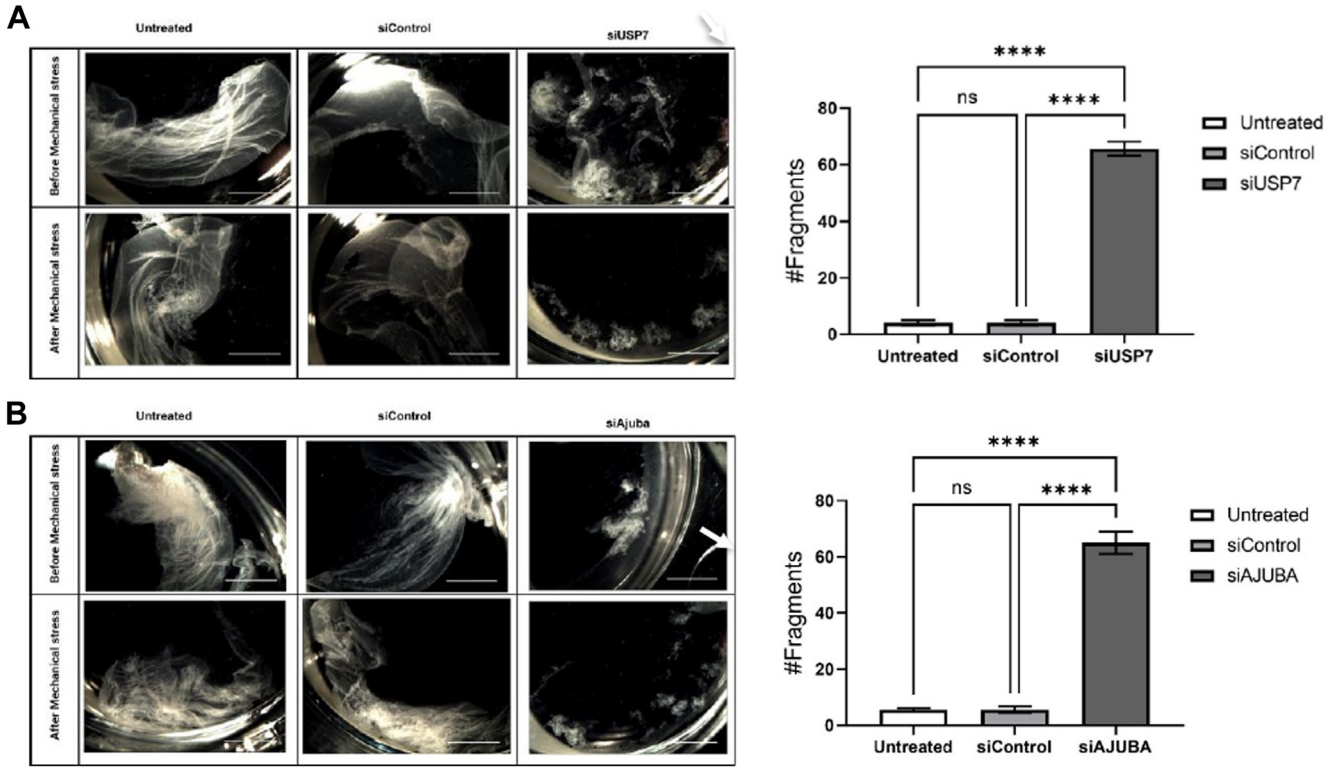

FIG. 6. **Mechanical stress analysis of cell-cell adhesion in LS88 cells.** *A*, monolayer cultures untreated or treated with siControl or siUSP7 were treated with dispase and incubated until the monolayer was detached from the culture surface, followed by shaking to induce fragmentation. The fragments were counted for all three conditions and the bar graph shows the average number of fragments. One-way ANOVA was used. ****$p < 0.0001$. Mean ± SD from three independent experiments. *Arrow* indicates increased fragmentation of monolayers following mechanical stress. Scale bar represents 5 mm. *B*, monolayer cultures untreated or treated with siControl or siAJuba were treated with dispase and incubated until the monolayer was detached from the culture surface, followed by shaking to induce fragmentation. The fragments were counted for all three conditions and the bar graph shows the average number of fragments. One-way ANOVA was used. ****$p < 0.0001$. Mean ± SD from three independent experiments. Arrow indicates increased fragmentation of monolayers following mechanical stress. Scale bar represents 5 mm.

most marked decreases in protein expression in Ajuba knockdown cells were observed for N-Cadherin (Fig. 8, *G* and *H*, consistent with previous reports (37, 38).

Taken together, these analyses suggest that USP7 plays an indirect role in regulating cell-cell adhesion through its interaction and regulation of the LIM domain protein Ajuba.

DISCUSSION

In this study, we used inducible knockdown proteomics to investigate novel interactions of the key deubiquitinase USP7 (Ubiquitin Specific Peptidase 7) in CRC. USP7 is known to promote cancer growth by upregulating several key cellular pathways, including the P53–MDM2 pathway (39) and Wnt/-catenin signaling (28). Its role as a regulator of these key cancer pathways has led to USP7 becoming an important therapeutic target and yet our wider understanding of its substrates, interactions, and functions is incomplete. We therefore used multimodal approaches to investigate USP7 and identified the Ajuba LIM domain protein as a novel USP7 interaction partner. We confirmed the substantial impact of USP7 on CRC cell viability in both 2D and 3D cultures, which is consistent with previous research that showed that USP7 inhibition using Parthenolide-reduced proliferation in HCT116 and SW480 CRC cells (16).

The effect of USP7 depletion was further validated in relation to cell sphere volume in LS88, LS174T, and DLD-1. This revealed significant decreases compared to the HEK 293T cell line. In addition, our study has used colony formation assay to examine the role of USP7 in the regulation of cell colonies, thereby revealing substantial cell colony inhibition in depleted USP7 CRC cells. These findings concur with previous research (40, 41). The current study verifies the importance of USP7 for cell survival in cases of CRC.

Cell adhesion plays an essential role in metastasis and cancer progression. One pathway that was enriched in our MS data for USP7 is cell adhesion. To characterize the USP7 role

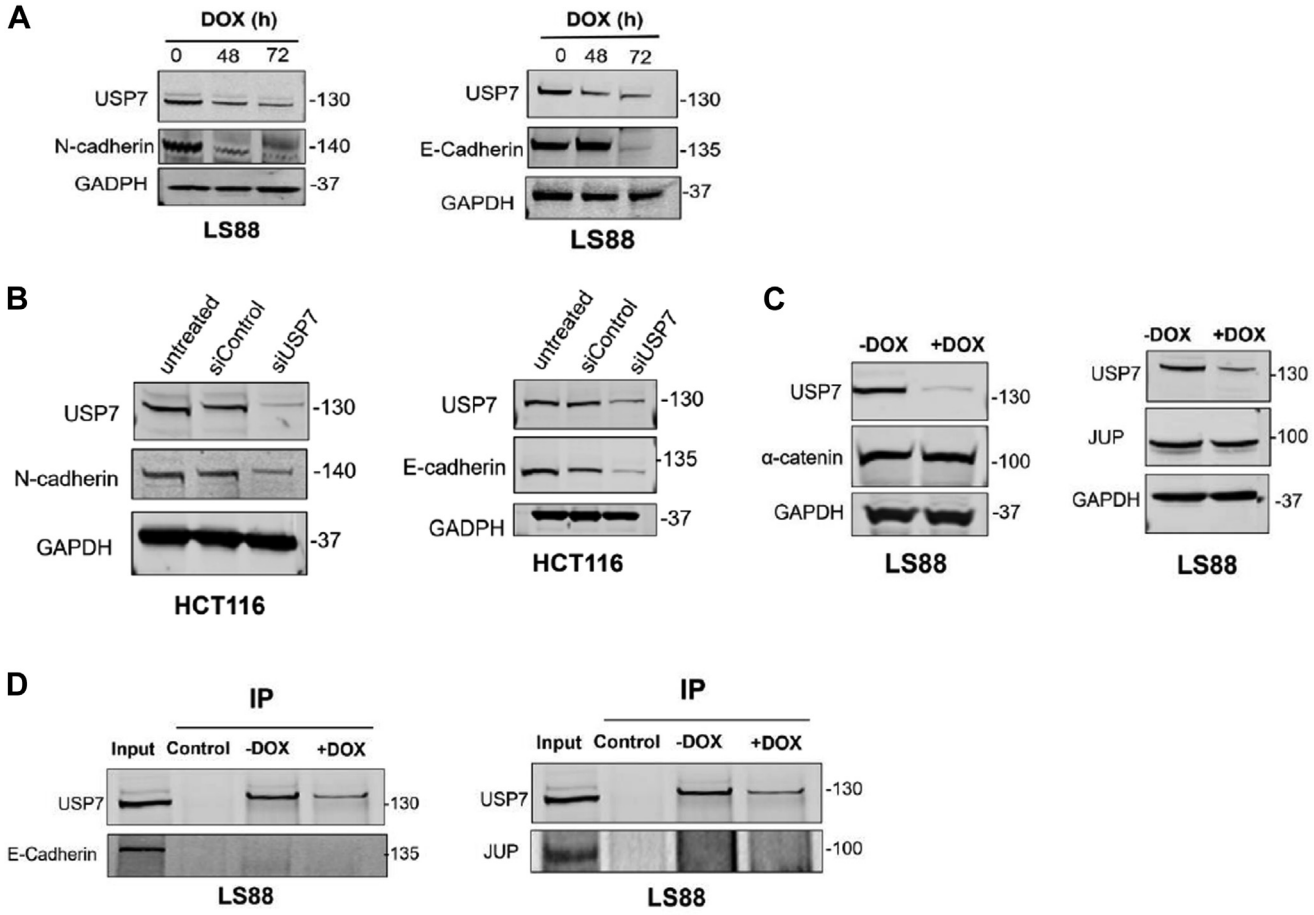

FIG. 7. **USP7 knockdown and effects on cadherin proteins and their substrates.** *A*, protein expression of N-cadherin and E-cadherin in LS88 cells treated with doxycycline (DOX) for the indicated time. GAPDH was used as a loading control. Adding doxycycline induces USP7 expression in LS88 cells. *B*, protein expression of N-cadherin and E-cadherin in HCT116 cells transfected with siUSP7 or siControl or left untreated. GAPDH was used as a loading control. *C*, α-catenin and γ-catenin expression were analyzed by Western blot. N = 3. GAPDH was used as a loading control. *D*, cell lysates from LS88 cells were immunoprecipitated with USP7; IgG antibodies followed by immunoblotting to examine the impact of USP7 knockdown on E-cadherin and γ-catenin (JUP).

in cell-cell junction, USP7 was knocked down, and the impacts on cell-cell adhesion were observed using dispase-based assay and mechanical stress in LS88. The results showed significant reductions in cell junctions. In the subsequent stage, we examined the master proteins that play a major role in cell adhesion in USP7-depleted cells in our cell model LS88 and other CRC cells. The findings confirmed the low expression of N-cadherin and E-cadherin when USP7 levels are reduced, although transcription levels must be measured in this context. However, no physical interactions were found between USP7, N-cadherin, E-cadherin, or JUP.

Many studies have shown that Ajuba acts as an oncogene due to its regulatory role in key signaling pathways, such as RAS/ERK, JAK/STAT, Wnt, and Hippo. The protein acts as a coregulator of main transcription factors, for example, Sp1, Snail, and nuclear hormone receptors. Amplified Ajuba expression has been found in viral types of tumors, suggesting its potential as a clinical prognostic and diagnostic marker (31). Ajuba is one of the proteins that has been linked to cell adhesion for over a decade (37, 42). The bioinformatics results emerging from our MS data indicated that Ajuba is a novel substrate for USP7 in our cell model. These findings were acquired in the lab using immunochemistry, immunoprecipitation, and siRNA oligos. The data confirmed the MS data, thereby indicating that Ajuba interacts directly with USP7 in CRC cells. We subsequently tested the central hypothesis that USP7 may influence cell-cell adhesion by regulating Ajuba protein levels. The results showed a reduction of N-cadherin and ITGB4 protein levels in Ajuba downregulated cells. These findings are consistent with earlier research (43). The results from the dispase-based essay in our lab demonstrated the high number of fragments in Ajuba knocked down cells. When combined, these findings suggest that the inhibition in the cell-cell

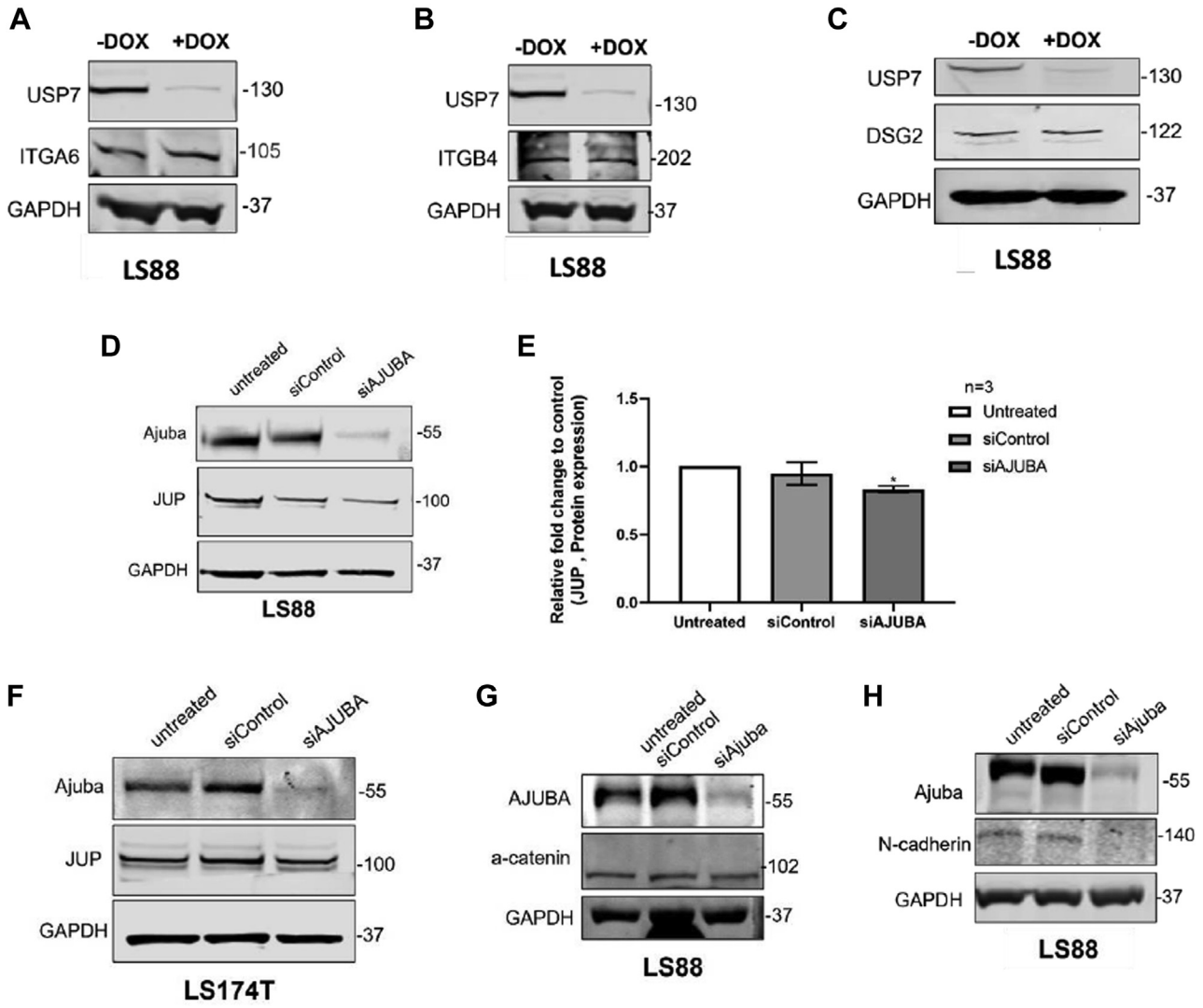

FIG. 8. **USP7 knockdown and effects on desmosome and hemidesmosome protein levels.** *A*, protein expression of ITGA6, (B) ITGB4, and (C) DSG2 were analyzed using Western blot. GAPDH was used as a loading control. *D*, LS88 cells were transfected with siControl and siAJUBA or left untreated; the cell lysates were subjected to Western blotting with indicated antibodies and graph (E) showing protein levels of JUP in the three conditions. The ordinary one-way-ANOVA was used from three independent experiments. The significant difference between the two groups untreated and siAjuba groups is $*p < 0.05$. Mean ± SD. *F*, Ajuba protein was knocked down in LS174T using siRNA and Western blot was performed using AJUBA and JUP antibodies. *G* and *H*, cell lysates from LS88 cell were subjected to immunoblotting with AJUBA and α -catenin and N-cadherin antibodies. GAPDH was used as a loading control.

junction in USP7-depleted cells may occur *via* Ajuba protein levels.

DATA AVAILABILITY

The mass-spectrometry data has been submitted to the PRIDE database with the following details: Project accession: PXD039488. All other data is provided within this paper and in the supplementary data.

Supplemental data—This article contains supplemental data.

Acknowledgments—The authors thank Professor Madelon Maurice (University Medical Center Utrecht) for kindly providing us with the LS88 cell-line.

Funding and additional information—R. M. E. acknowledges Medical Research Council (MR/S01411X/1) and European Commission FP7 ("Oncoprotnet") for funding; Y. W. acknowledges Medical Research Council (MR/S025480/1).

Author contributions—A. A.-E., B. C., P. S., Y. W., and R. M. E. writing–review and editing; A. A.-E. and R. M. E. writing–original draft; A. A.-E., S. W., methodology; A. A.-E., B. D.,

B. C., investigation; P. S., Y. W., and R. M. E. supervision; P. S. and R. M. E. project administration; R. M. E. funding acquisition; R. M. E. conceptualization.

Conflicts of interest—The authors declare that they have no conflicts of interest with the contents of this article.

Abbreviations—The abbreviations used are: CRC, colorectal cancer; BSA, bovine serum albumin; DUB, deubiquitinating enzyme; FDR, false discovery rate; HBSS, Hanks' Balanced Salt Solution; IgG, immunoglobulin G; MS, mass spectrometry; PCA, principal component analysis; USP7, ubiquitin-specific protease 7.

Received February 23, 2024, and in revised form, November 4, 2024 Published, MCPRO Papers in Press, November 9, 2024, https://doi.org/10.1016/j.mcpro.2024.100878

REFERENCES

1. Dewson, G., Eichhorn, P. J. A., and Komander, D. (2023) Deubiquitinases in cancer. *Nat. Rev. Cancer* **23**, 842–862
2. Bushman, J. W., Donovan, K. A., Schauer, N. J., Liu, X., Hu, W., Varca, A. C., *et al*. (2021) Proteomics-based identification of DUB substrates using selective inhibitors. *Cell Chem. Biol.* https://doi.org/10.1016/j.chembiol.2020.09.005
3. Reyes-Turcu, F. E., Ventii, K. H., and Wilkinson, K. D. (2009) Regulation and cellular roles of ubiquitin-specific deubiquitinating enzymes. *Annu. Rev. Biochem.* **78**, 363–397
4. Sowa, M. E., Bennett, E. J., Gygi, S. P., and Harper, J. W. (2009) Defining the human deubiquitinating enzyme interaction landscape. *Cell* **138**, 389–403
5. Song, L., and Rape, M. (2008) Reverse the curse-the role of deubiquitination in cell cycle control. *Curr. Opin. Cell Biol.* https://doi.org/10.1016/j.ceb.2008.01.012
6. Daniel, J. A., and Grant, P. A. (2007) Multi-tasking on chromatin with the SAGA coactivator complexes. *Mutat. Res. - Fundam. Mol. Mech. Mutagen* **618**. https://doi.org/10.1016/j.mrfmmm.2006.09.008
7. Kennedy, R. D., and D'Andrea, A. D. (2005) The Fanconi Anemia/BRCA pathway: new faces in the crowd. *Genes Dev.* https://doi.org/10.1101/gad.1370505
8. Fischer, J. A. (2003) Deubiquitinating enzymes: their roles in development, differentiation, and disease. *Int. Rev. Cytol.* **229**. https://doi.org/10.1016/S0074-7696(03)29002-1
9. Shanmugham, A., and Ovaa, H. (2008) DUBs and disease: activity assays for inhibitor development. *Curr. Opin. Drug Discov. Devel.* **11**, 688–696
10. Nijman, S. M. B., Luna-Vargas, M. P. A., Velds, A., Brummelkamp, T. R., Dirac, A. M. G., Sixma, T. K., *et al*. (2005) A genomic and functional inventory of deubiquitinating enzymes. *Cell*. https://doi.org/10.1016/j.cell.2005.11.007
11. Bedford, L., Lowe, J., Dick, L. R., Mayer, R. J., and Brownell, J. E. (2011) Ubiquitin-like protein conjugation and the ubiquiting-proteasome system as drug targets. *Nat. Rev. Drug Discov*. https://doi.org/10.1038/nrd3321
12. Nicholson, B., Marblestone, J. G., Butt, T. R., and Mattern, M. R. (2007) Deubiquitinating enzymes as novel anticancer targets. *Future Oncol.* https://doi.org/10.2217/14796694.3.2.191
13. Saridakis, V., Sheng, Y., Sarkari, F., Holowaty, M. N., Shire, K., Nguyen, T., *et al*. (2005) Structure of the p53 binding domain of HAUSP/USP7 bound to Epstein-Barr nuclear antigen 1 implications for EBV-mediated immortalization. *Mol. Cell* **18**, 25–36
14. Al-Eidan, A., Wang, Y., Skipp, P., and Ewing, R. M. (2022) The USP7 protein interaction network and its roles in tumorigenesis. *Genes Dis.* **9**, 41
15. Saha, G., Roy, S., Basu, M., and Ghosh, M. K. (2023) USP7 - a crucial regulator of cancer hallmarks. *Biochim. Biophys. Acta Rev. Cancer* **1878**, 188903
16. Li, X., Kong, L., Yang, Q., Duan, A., Ju, X., Cai, B., *et al*. (2020) Parthenolide inhibits ubiquitin-specific peptidase 7 (USP7), Wnt signaling, and colorectal cancer cell growth. *J. Biol. Chem.* **295**, 3576
17. Becker, K., Marchenko, N. D., Palacios, G., and Moll, U. M. (2008) A role of HAUSP in tumor suppression in a human colon carcinoma xenograft model. *Cell Cycle*. https://doi.org/10.4161/cc.7.9.5756
18. Zhi, Y., Shoujun, H., Yuanzhou, S., Haijun, L., Yume, X., Kai, Y., *et al*. (2012) STAT3 repressed USP7 expression is crucial for colon cancer development. *FEBS Lett.* **586**, 3013–3017
19. Sho, S., CM, C., P, W., MM, R., and JS, T. (2017) A prognostic mutation panel for predicting cancer recurrence in stages II and III colorectal cancer. *J. Surg. Oncol.* **116**, 996–1004
20. Kessler, B. M., Fortunati, E., Melis, M., Pals, C. E. G. M., Clevers, H., and Maurice, M. M. (2007) Proteome changes induced by knock-down of the deubiquitylating enzyme HAUSP/USP7. *J. Proteome Res.* **6**, 4163–4172
21. Tsherniak, A., Vazquez, F., Montgomery, P. G., Weir, B. A., Kryukov, G., Cowley, G. S., *et al*. (2017) Defining a cancer dependency map. *Cell* **170**, 564–576.e16
22. Huang, D. W., Sherman, B. T., and Lempicki, R. A. (2008) Systematic and integrative analysis of large gene lists using DAVID bioinformatics resources. *Nat. Protoc.* **41**, 44–57
23. Ge, S. X., Jung, D., Jung, D., and Yao, R. (2020) ShinyGO: a graphical gene-set enrichment tool for animals and plants. *Bioinformatics* **36**. https://doi.org/10.1093/bioinformatics/btz931
24. Zhou, Y., Zhou, B., Pache, L., Chang, M., Khodabakhshi, A. H., Tanaseichuk, O., *et al*. (2019) Metascape provides a biologist-oriented resource for the analysis of systems-level datasets. *Nat. Commun.* **10**, 1523
25. Meulmeester, E., Maurice, M. M., Boutell, C., Teunisse, A. F. A. S., Ovaa, H., Abraham, T. E., *et al*. (2005) Loss of HAUSP-mediated deubiquitination contributes to DNA damage-induced destabilization of Hdmx and Hdm2. *Mol. Cell* **18**, 565–576
26. Onoda, T., Ono, T., Dhar, D. K., Yamanoi, A., Fujii, T., and Nagasue, N. (2004) Doxycycline inhibits cell proliferation and invasive potential: combination therapy with cyclooxygenase-2 inhibitor in human colorectal cancer cells. *J. Lab. Clin. Med.* **143**, 207–216
27. Sagar, J., Sales, K., Taanman, J. W., Dijk, S., and Winslet, M. (2010) Lowering the apoptotic threshold in colorectal cancer cells by targeting mitochondria. *Cancer Cell Int.* https://doi.org/10.1186/1475-2867-10-31
28. Novellasdemunt, L., Foglizzo, V., Cuadrado, L., Antas, P., Kucharska, A., Encheva, V., *et al*. (2017) USP7 is a tumor-specific WNT activator for APC-mutated colorectal cancer by mediating β-catenin deubiquitination. *Cell Rep.* **21**, 612–627
29. Liu, X., Yang, X., Li, Y., Zhao, S., Li, C., Ma, P., *et al*. (2016) Trip12 is an E3 ubiquitin ligase for USP7/HAUSP involved in the DNA damage response. *FEBS Lett.* **590**, 4213–4222
30. Zaman, M. M.-U., Nomura, T., Takagi, T., Okamura, T., Jin, W., Shinagawa, T., *et al*. (2013) Ubiquitination-deubiquitination by the TRIM27-USP7 complex regulates tumor necrosis factor alpha-induced apoptosis. *Mol. Cell. Biol.* **33**, 4971–4984
31. Jia, H., Peng, H., and Hou, Z. (2020) Ajuba: an emerging signal transducer in oncogenesis. *Pharmacol. Res.* https://doi.org/10.1016/j.phrs.2019.104546
32. Thul, P. J., Akesson, L., Wiking, M., Mahdessian, D., Geladaki, A., Ait Blal, H., *et al*. (2017) A subcellular map of the human proteome. *Science* **356**. https://doi.org/10.1126/science.aal3321
33. Zapata, J. M., Pawlowski, K., Haas, E., Ware, C. F., Godzik, A., and Reed, J. C. (2001) A diverse family of proteins containing tumor necrosis factor receptor-associated factor domains. *J. Biol. Chem.* **276**, 24242–24252
34. Herbst, A., Jurinovic, V., Krebs, S., Thieme, S. E., Blum, H., Göke, B., *et al*. (2014) Comprehensive analysis of β-catenin target genes in colorectal carcinoma cell lines with deregulated Wnt/β-catenin signaling. *BMC Genomics* **15**. https://doi.org/10.1186/1471-2164-15-74
35. Ji, L., Lu, B., Zamponi, R., Charlat, O., Aversa, R., Yang, Z., *et al*. (2019) USP7 inhibits Wnt/β-catenin signaling through promoting stabilization of Axin. *Nat. Commun.* https://doi.org/10.1038/s41467-019-12143-3
36. Green, K. J., and Jones, J. C. R. (1996) Desmosomes and hemidesmosomes: structure and function of molecular components. *FASEB J.* **10**, 871–881
37. Marie, H., Pratt, S. J., Betson, M., Epple, H., Kittler, J. T., Meek, L., *et al*. (2003) The LIM protein Ajuba is recruited to cadherin-dependent cell junctions through an association with α-catenin. *J. Biol. Chem.* **278**, 1220–1228
38. Sarpal, R., Yan, V., Kazakova, L., Sheppard, L., Yu, J. C., Fernandez-Gonzalez, R., *et al*. (2019) Role of α-Catenin and its mechanosensing properties in regulating Hippo/YAP-dependent tissue

growth. *PLoS Genet.* **15**. https://doi.org/10.1371/JOURNAL.PGEN.1008454
39. Harakandi, C., Nininahazwe, L., Xu, H., Liu, B., He, C., Zheng, Y. C., *et al*. (2021) Recent advances on the intervention sites targeting USP7-MDM2-p53 in cancer therapy. *Bioorg. Chem.* **116**. https://doi.org/10.1016/J.BIOORG.2021.105273
40. Behan, F. M., Iorio, F., Picco, G., Gonçalves, E., Beaver, C. M., Migliardi, G., *et al*. (2019) Prioritization of cancer therapeutic targets using CRISPR–Cas9 screens. *Nature* **568**. https://doi.org/10.1038/s41586-019-1103-9
41. Hayal, T. B., Doğan, A., Şişli, H. B., Kiratli, B., and Şahin, F. (2020) Ubiquitin-specific protease 7 downregulation suppresses breast cancer *in vitro*. *Turk. J. Biol.* **44**, 145
42. Nola, S., Daigaku, R., Smolarczyk, K., Carstens, M., Martin-Martin, B., Longmore, G., *et al*. (2011) Ajuba is required for Rac activation and maintenance of E-cadherin adhesion. *J. Cell Biol.* **195**, 855
43. Peifer, M., and Wleschaus, E. (1990) The segment polarity gene armadillo encodes a functionally modular protein that is the Drosophila homolog of human plakoglobin. *Cell* **63**, 1167–1178